CrystEngComm

ROYAL SOCIETY OF CHEMISTRY

COMMUNICATION

View Article Online
View Journal | View Issue

Cite this: *CrystEngComm*, 2024, **26**, 6003

Received 28th August 2024,
Accepted 9th October 2024

DOI: 10.1039/d4ce00861h

rsc.li/crystengcomm

Hydrogen storage of commercially scalable CALF-20: a study at cryogenic and near-ambient temperatures†

Ashley L. Sutton, *[a] M. Munir Sadiq, [a] James I. Mardel[a] and Matthew R. Hill [ab]

The hydrogen storage capabilities of the metal–organic framework (MOF) CALF-20 are examined experimentally with both cryogenic and near-ambient temperatures. This framework has a pore size that is nearly ideal for cryogenic hydrogen storage. Density functional theory (DFT) studies provide insights into the hydrogen binding sites within CALF-20.

Introduction

Metal–organic frameworks (MOFs) are a class of porous materials, renowned for unmatched surface areas and highly customisable structures.[1–3] They find applications ranging from gas storage[4–6] and separation,[7–9] catalysis[10–12] and drug delivery.[13–15] Hydrogen storage is a particular role that has gained much attention.[16–18] MOFs can adsorb significant quantities of hydrogen gas due to their high surface areas and the inclusion of functionalities such as open metal sites.[19–22] Hydrogen storage may be critical for addressing one of the world's most pressing challenges – transitioning to a net zero carbon economy.[23]

Efficient hydrogen storage systems are essential for the widespread adoption of hydrogen as a net zero carbon energy carrier, particularly for on-board vehicular applications.[24] MOFs have the potential to meet the United States Department of Energy (US DOE) on-board hydrogen storage system targets of 6.5 wt% and 50 g L^{-1}.[25] However, many challenges are yet to be overcome, including the design of MOFs that can operate within the desired regime of −50 C to +50 C, material stability under application conditions, and production scale-up of the suitable MOF. CALF-20, [Zn_2(1,2,4-triazolate)$_2$(oxalate)], shown in Fig. 1, is a MOF most famously known for its selective CO_2 adsorption in the application of flue gas capture.[26] CALF-20 has been shown to meet many of the challenges associated with commercial scale-up.[26] It has also been shown to be a very robust material that can withstand harsh conditions, including steam, wet acid gases and direct combustion flue gas.[26] These qualities make CALF-20 an attractive material for other applications. There have been several significant follow-up studies into CALF-20. These studies have been computationally based and have demonstrated that a) diffusion of guest CO_2 and H_2O molecules within CALF-20 occurs *via* an abnormal mechanism[27,28] and b) CALF-20 shows flexibility upon guest loading.[29] These finding will no doubt play a significant role in designing next-generation materials. Finally, its versatility goes beyond flue gas capture and includes separation of Xe/Kr/N_2.[30]

Its structure comprises one crystallographically unique Zn(II) centre, which is five coordinate with a distorted trigonal bipyramidal geometry. There are no open metal sites within the structure. Layers of zinc(II) ions are bridged by 1,2,4-

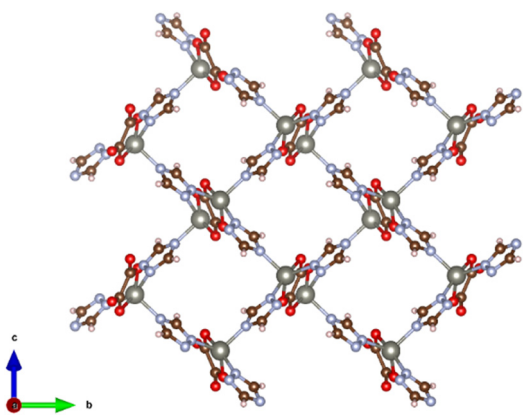

Fig. 1 Ball and stick illustration of CALF-20, viewed along the *a*-axis channel direction. Grey represents Zn, red represents O, blue represents N, and off-white represents H.

[a] *Manufacturing, CSIRO, Private Bag 33, Clayton South MDC, Victoria 3169, Australia. E-mail: ashley.sutton@csiro.au*
[b] *Department of Chemical and Biological Engineering, Monash University, Clayton, Vic 3168, Australia*

† Electronic supplementary information (ESI) available: Synthetic and characterization details. See DOI: https://doi.org/10.1039/d4ce00861h

triazolate ligands, which form porous 2D $[Zn_2(1,2,4\text{-triazolate})_2]^{2+}$ sheets. These sheets are connected at the zinc ions to form a porous 3D MOF by oxalate anions. Notably, CALF-20 features channels with relatively small dimensions, the largest of which is located along the *a*-axis, measuring just ~2.8 Å by ~3.2 Å, accounting for van der Waals radii. This is well suited for hydrogen uptake as H_2 possesses a kinetic diameter of 2.89 Å.[31]

We investigate CALF-20 for hydrogen storage applications. Its cryogenic storage ability is compared to that of near-ambient temperature storage. Density functional theory (DFT) studies elucidate potential hydrogen binding sites within CALF-20.

Results & discussion

CALF-20 was synthesised according to a modified literature procedure.[32] Powder X-ray diffraction (Fig. S1†) indicated the material was of the β-phase of CALF-20, a consequence of the material being exposed to humid air.[33] Prior to gas sorption, the material was activated. Application of vacuum has been shown to transform the β-phase back to the α-phase. Gas sorption with N_2 at 77 K (Fig. S2†) revealed a Brunauer–Emmett–Teller (BET) surface of 513 $m^2\ g^{-1}$, consistent with the literature.[30]

Low-pressure H_2 isotherms were conducted to provide insights into hydrogen uptake at cryogenic temperatures. Measurements at 77 K revealed CALF-20 uptakes 20.5 g L^{-1} or 1.28 wt% of H at 1 bar as shown in Fig. 2. Previously, grand canonical Monte Carlo (GCMC) of over 140 000 hypothetical MOFs revealed the vast majority have a volumetric uptake between 10 to 30 g L^{-1} at 77 K and 2 bar.[34] Further, there is a relationship between H_2 uptake and surface area. CALF-20, with a surface area of ~500 $m^2\ g^{-1}$ and adsorption of 20.5 g L^{-1} would be in the top 10% of MOFs with a similar surface area. Given that CALF-20 can be produced at scale and is chemically robust it is an interesting material for hydrogen storage.

We compare CALF-20's working capacity with MOF-5 under pressure swing conditions 100 bar to 5 bar at 77 K using Monte Carlo (see ESI† for details). MOF-5 has been considered the benchmark material for cryogenic hydrogen storage. It can deliver 31 g L^{-1} under the above conditions,[35] in contrast to CALF-20 which can only deliver 13 g L^{-1}. Using a temperature–pressure swing system (77 K/100 bar to 160 K/5 bar) however dramatically raises the working capacity of CALF-20 to 33 g L^{-1} (see ESI†). This highlights the need to consider the optimal working conditions for the material at hand.

Measurements at 87 K with H_2 allowed for calculating the hydrogen binding enthalpy *via* the Clausius–Clapeyron equation. The measured initial binding enthalpy was consistent with physisorption at −7.9 kJ mol^{-1}. While we present this initial it is important to contrast it with a binding enthalpy across a range typically associated with high surface loadings, which are likely to be experienced in real-world hydrogen storage applications. We note to meet the US DOE system target of 6.5 wt%, would require a MOF to store at least 35 mmol H_2 per g. The binding enthalpy for CALF-20 is relatively constant up to a loading of least 4.0 mmol H_2 per g (see Fig. 3, blue line) and has an average enthalpy of −8.1 kJ mol^{-1} between loadings of 0.05 mmol H_2 per g and 3.00 mmol H_2 per g. Other MOFs display this type of behaviour. For instance, Ni_2(m-dobdc),[36] has an average binding enthalpy of −10.7 kJ mol^{-1} across the range of 0.01–4.0 mmol H_2 per g, its binding enthalpy later drops once the Ni open metal sites become saturated.

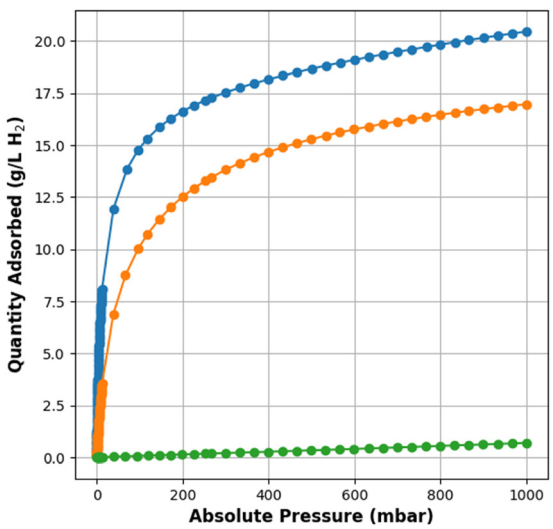

Fig. 2 Low pressure hydrogen isotherms for CALF-20 obtained at cryogenic 77 K (blue), 87 K (orange) and 298 K (green). Volumetric uptake is based on a crystallographic density of 1.60 g cm^{-3}.

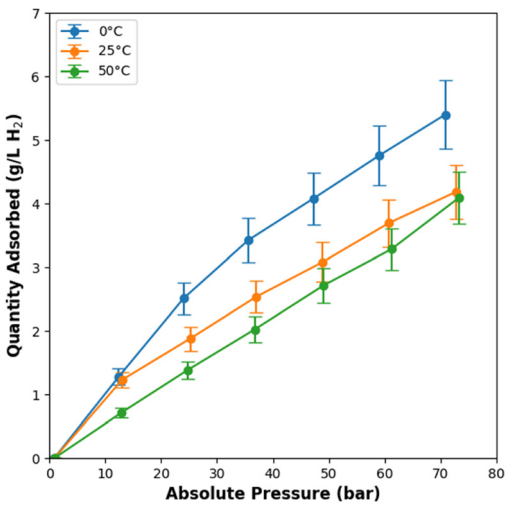

Fig. 3 Binding enthalpies (kJ mol^{-1}) as a function of H_2 loading (mmol g^{-1}) for a range of frameworks including CALF-20 (blue). Frameworks include; NU-2100 (orange),[22] Ni_2(m-dobdc) (green),[36] Co-BTT (red).[37] Inset: Average binding enthalpy (kJ mol^{-1}) as function of cost (USD$ per kg), target zone −15 to −25 kJ mol^{-1} at cost of less than USD$ 10 000 per kg.

Saturation occurs significantly sooner for NU-2100,[22] which has a record high initial binding enthalpy of −32 kJ mol^{-1}, sharply dropping to −6.3 kJ mol^{-1} at just 0.25 mmol H_2 per g (see Fig. 3, orange line). This results in an average binding enthalpy of just −9.2 kJ mol^{-1} across the 0.01–3.00 mmol H_2 per g range. Thus, the average binding enthalpy is just 1.1 kJ mol^{-1} more favourable than that of CALF-20. Such a slight difference in average binding enthalpy indicates CALF-20 is competitive with world-leading MOFs on this metric. Ideally, a MOF material will be developed in which the average binding enthalpy is between −15 and −25 kJ mol^{-1} across the loading range of 0.01–6.50 mmol H_2 per g.

This analysis can be extended further by examining the cost of the MOF material associated with its average binding enthalpy, *i.e.* examining the price performance ratio. CALF-20 has the lowest cost of all MOFs examined at just USD$ 29 per kg, whilst NU-2100 has the highest cost at USD$ 139 per kg (see ESI†). The price performance ratio of CALF-20 is approximately 4.2 times better than NU-2100, indicating superior cost-effectiveness and efficiency in applications where high performance is needed.

Ambient temperature (298 K) reveals a significant drop in the quantity of H_2 adsorbed with a total uptake of 0.69 g L^{-1} at 1 bar, highlighting the challenges faced with near-ambient temperature hydrogen storage.

MOFs developed for near-ambient temperature storage, which all employ open metal sites, have the following total capacities; 7.2 g L^{-1} for Cu_2(BBTA),[22] 10.7 g L^{-1} for $V_2Cl_{2.8}$(bttd)[21] and 11.9 g L^{-1} for Ni_2(m-dobdc)[36] at 298 K and 100 bar.

The binding enthalpy of −7.9 kJ mol^{-1} for CALF-20 is not ideal for near-ambient hydrogen storage. However, we still opted to explore its hydrogen storage capabilities between 1 and 75 bar and 273 K and 323 K, given its cost-effectiveness, scalability and robustness. At room temperature CALF-20 can uptake 4.2 g L^{-1} of hydrogen at 73 bar (Fig. 4). Using a fit of this uptake, an extrapolated value of 5.8 g L^{-1} would be achieved at 100 bar. Its gravimetric uptake is 0.36 wt% under these conditions. It is apparent that CALF-20 has a rather low gravimetric uptake at 298 K and 100 bar, but its volumetric uptake is considerable. This may be considered favourable given the space constraints for on-board vehicular storage.[36,38,39]

In real-world scenarios, working capacities are likely to be more important than total adsorption.[40] The US DOE system targets have specified a desire for a minimum working pressure of 5 bar within the operating conditions of −50 C to +50 C.[25] This opens the possibility of temperature–pressure swing adsorption. With grand canonical Monte calculations (GCMC) (see ESI†) it is possible to determine the uptake under this scenario (see Fig. S3†). An on-board hydrogen storage device filled with MOF is likely to operate between a full state at 100 bar and 223 K and an empty state at 5 bar and 323 K. Under such conditions CALF-20 would have a working capacity of 10.5 g L^{-1}. This is well below the US DOE system target of 50 g L^{-1}, but slightly better than a conventional hydrogen tank under the same conditions.

These results highlight the need to understand further the beneficial interactions that occur between H_2 and CALF-20, which will help to develop materials that can achieve the US DOE system targets.

To bridge this knowledge gap, we employed DFT to probe the structure of CALF-20 and the interactions that lead to a binding enthalpy of −7.9 kJ mol^{-1}. Specifically, our investigation into H_2 uptake in CALF-20 involved calculations to elucidate the storage mechanism. Initially the structure of CALF-20 was optimized to a minimum energy state.

Searches were performed to identify the most favourable energy-binding site within the frozen framework. It should be noted that very recently CALF-20 was shown to have flexible behaviour upon guest loading[29] – future studies to explore

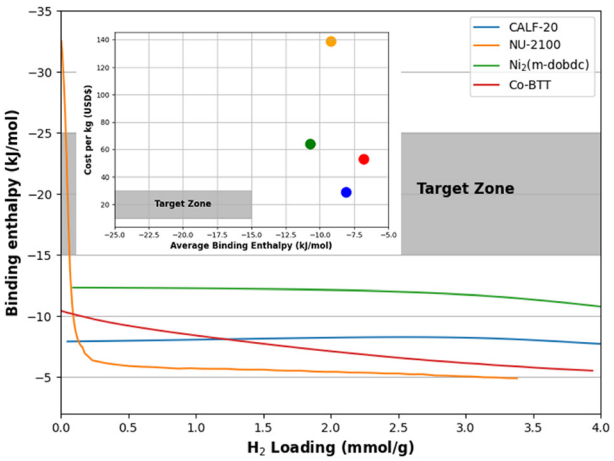

Fig. 4 High pressure hydrogen isotherms for CALF-20 obtained at near-ambient temperatures. Volumetric uptake is based on a crystallographic density of 1.60 g cm^{-3}.

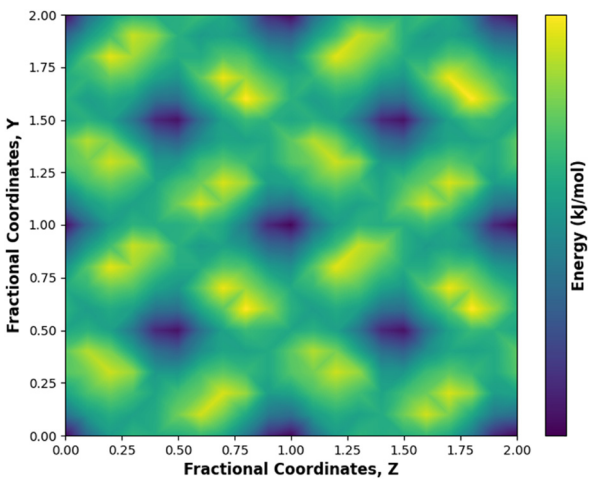

Fig. 5 2D heatmap looking down the pores of CALF-20, illustrating the binding enthalpy as a function of fractional coordinates for a 2 × 2 × 2 supercell at an X-ray crystal coordinate of 0.0. Unfavourable sites are depicted in yellow, typically corresponding to the location of framework atoms, while the most favourable sites are shown in blue.

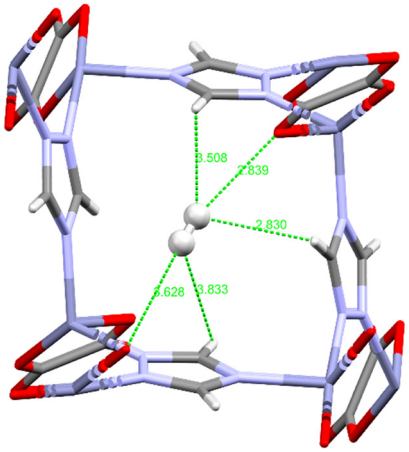

Fig. 6 Structure showing the most favourable binding site for H_2 within CALF-20.

the effect hydrogen has on a dynamic framework would be of interest. These efforts revealed a distinct site within CALF-20. This optimal binding site is depicted through a contour plot of binding energy, Fig. 5 and a clear visualisation of the adsorption site in Fig. 6.

The binding enthalpy at this preferred site is −8.5 kJ mol^{-1}, which correlates well with the binding energy determined experimentally, validating our computational approach. It is important to understand the nature and geometry of H_2 interactions within pore architectures such as those found in CALF-20. An important aspect of the structural calculations undertaken in this study involves examining the short contacts between H_2 and the framework. In CALF-20, H_2 sits diagonally within the pore, with each H atom of the H_2 pointing towards the oxygen of the C═O of an oxalate ligand with one end considerably close than the other, 2.84 Å *vs.* 3.83 Å. This favourable interaction, presumably facilitated by dipole–dipole forces, given the polar nature of the C═O bond contributes to stabilising the H_2 binding site. Additional short contacts range from 2.83 to 3.51 Å between the C–H of triazole rings and H_2. Whilst most of these interactions are longer than the oxalate–H_2 contact, they are influential van der Waals interactions that also help to stabilize the H_2 molecule binding site. Understanding these interactions is crucial for engineering MOFs with significant storage capacity, especially at near-ambient temperatures.

Conclusions

Transitioning away from carbon-based energy carriers is a significant challenge the world faces. The MOF community, particularly those exploring hydrogen storage, have a key role in this challenge. The US DOE has set demanding system targets for near-ambient temperature hydrogen storage. We explored the robust and highly scalable MOF, CALF-20, for cryogenic and near-ambient temperature hydrogen storage. CALF-20 shows a significant uptake of 20.5 g L^{-1} of hydrogen at 77 K and 1 bar. Its initial binding enthalpy is −7.9 kJ mol^{-1}, indicative of physisorption. Further, its average binding enthalpy of −8.1 kJ mol^{-1} on loadings between 0.05 mmol H_2 per g and 3.00 mmol H_2 per g is competitive with recording leading MOFs in the field on this metric. At ambient temperature the uptake is 5.8 g L^{-1} at 100 bar. With its working capacity improving to 10.5 g L^{-1} between 323 K and 5 bar and 223 K and 100 bar. DFT studies revealed a binding site consistent in energy with experimental methods. The pore architecture is directly responsible for the H_2 binding with several short-range contacts and extensive dipole–dipole and van der Waals interactions. Although the small pores of CALF-20 provide increased binding enthalpy over more traditional large-pore based MOFs, it still fails to achieve the US DOE targets. Conceivably a small pore aperture framework with increased surface area (*i.e.* >1000 m^2 g^{-1}) would yield more favourable results.

Data availability

The data supporting this article have been included as part of the ESI.†

Conflicts of interest

There are no conflicts to declare.

Acknowledgements

This project was supported by resources and expertise provided by CSIRO IMT Scientific Computing.

Notes and references

1 H. Li, M. Eddaoudi, M. O'Keefe and O. M. Yaghi, *Nature*, 1999, **402**, 276–279.
2 H. Furukawa, K. E. Cordova, M. O'Keeffe and O. M. Yaghi, *Science*, 1979, **2013**, 341.
3 J. L. C. Rowsell and O. M. Yaghi, *Microporous Mesoporous Mater.*, 2004, **73**, 3–14.
4 H. Li, L. Li, R. B. Lin, W. Zhou, Z. Zhang, S. Xiang and B. Chen, *EnergyChem*, 2019, **1**, 1–78.
5 B. Li, H. M. Wen, W. Zhou and B. Chen, *J. Phys. Chem. Lett.*, 2014, **5**, 3468–3479.
6 W. Fan, X. Zhang, Z. Kang, X. Liu and D. Sun, *Coord. Chem. Rev.*, 2021, **443**, 213968.
7 J. Duan, Y. Pan, G. Liu and W. Jin, *Curr. Opin. Chem. Eng.*, 2018, **20**, 122–131.
8 D. M. D'Alessandro, B. Smit and J. R. Long, *Angew. Chem., Int. Ed.*, 2010, **49**, 6058–6082.
9 Z. R. Herm, J. A. Swisher, B. Smit, R. Krishna and J. R. Long, *J. Am. Chem. Soc.*, 2011, **133**, 5664–5667.
10 V. Pascanu, G. G. Miera, A. K. Inge and B. Martín-Matute, *J. Am. Chem. Soc.*, 2019, **141**, 7223–7234.
11 J. Liu, L. Chen, H. Cui, J. Zhang, L. Zhang and C. Y. Su, *Chem. Soc. Rev.*, 2014, **43**, 6011–6061.

12 T. Zhang and W. Lin, *Chem. Soc. Rev.*, 2014, **43**, 5982–5993.
13 H. D. Lawson, S. P. Walton and C. Chan, *ACS Appl. Mater. Interfaces*, 2021, **13**, 7004–7020.
14 M. Moharramnejad, A. Ehsani, M. Shahi, S. Gharanli, H. Saremi, R. E. Malekshah, Z. S. Basmenj, S. Salmani and M. Mohammadi, *J. Drug Delivery Sci. Technol.*, 2023, **81**, 104285.
15 S. Mallakpour, E. Nikkhoo and C. M. Hussain, *Coord. Chem. Rev.*, 2022, **451**, 214262.
16 M. P. Suh, H. J. Park, T. K. Prasad and D. W. Lim, *Chem. Rev.*, 2012, **112**, 782–835.
17 S. P. Shet, S. S. Priya, K. Sudhakar and M. Tahir, *Int. J. Hydrogen Energy*, 2021, **46**, 11782–11803.
18 A. Ahmed and D. J. Siegel, *Patterns*, 2021, **2**, 100291.
19 M. Hirscher and B. Panella, *J. Alloys Compd.*, 2005, **404–406**, 399–401.
20 R. Balderas-Xicohténcatl, P. Schmieder, D. Denysenko, D. Volkmer and M. Hirscher, *Energy Technol.*, 2018, **6**, 510–512.
21 D. E. Jaramillo, H. Z. H. Jiang, H. A. Evans, R. Chakraborty, H. Furukawa, C. M. Brown, M. Head-Gordon and J. R. Long, *J. Am. Chem. Soc.*, 2021, **143**, 6248–6256.
22 D. Sengupta, P. Melix, S. Bose, J. Duncan, X. Wang, M. R. Mian, K. O. Kirlikovali, F. Joodaki, T. Islamoglu, T. Yildirim, R. Q. Snurr and O. K. Farha, *J. Am. Chem. Soc.*, 2023, **145**, 20492–20502.
23 K. Jha, P. Gulati and T. K. Uma, *Recent Advances in Sustainable Technologies: Select Proceedings of ICAST 2020*, 2020.
24 J. A. Gómez and D. M. F. Santos, *Designs*, 2023, **7**, 97.
25 US Department of Energy, *Target Explanation Document: Onboard Hydrogen Storage for Light-Duty Fuel Cell Vehicles*, 2017.
26 J.-B. Lin, T. T. T. Nguyen, R. Vaidhyanathan, J. Burner, J. M. Taylor, H. Durekova, F. Akhtar, R. K. Mah, O. Ghaffari-Nik, S. Marx, N. Fylstra, S. S. Iremonger, K. W. Dawson, P. Sarkar, P. Hovington, A. Rajendran, T. K. Woo and G. K. H. Shimizu, *Science*, 1979, **2021**(374), 1464–1469.
27 Y. Magnin, E. Dirand, G. Maurin and P. L. Llewellyn, *ACS Appl. Nano Mater.*, 2023, **6**, 19963–19971.
28 C. H. Ho and F. Paesani, *ACS Appl. Mater. Interfaces*, 2023, **15**, 48287–48295.
29 R. Oktavian, R. Goeminne, L. T. Glasby, P. Song, R. Huynh, O. T. Qazvini, O. Ghaffari-Nik, N. Masoumifard, J. L. Cordiner, P. Hovington, V. Van Speybroeck and P. Z. Moghadam, *Nat. Commun.*, 2024, **15**, 1–10.
30 Y. Wei, F. Qi, Y. Li, X. Min, Q. Wang, J. Hu and T. Sun, *RSC Adv.*, 2022, **12**, 18224–18231.
31 A. F. Ismail, K. C. Khulbe and M. Takeshi, *Gas Separation Membranes: Polymeric and Inorganic*, Springer, 2015.
32 T. T. T. Nguyen, J. Bin Lin, G. K. H. Shimizu and A. Rajendran, *Chem. Eng. J.*, 2022, **442**, 136263.
33 Z. Chen, C. H. Ho, X. Wang, S. M. Vornholt, T. M. Rayder, T. Islamoglu, O. K. Farha, F. Paesani and K. W. Chapman, *ACS Mater. Lett.*, 2023, **5**, 2942–2947.
34 N. S. Bobbitt, J. Chen and R. Q. Snurr, *J. Phys. Chem. C*, 2016, **120**, 27328–27341.
35 D. J. Siegel, A. Ahmed, A. Matzger, A. Shresth and A. Wong-Foy, *Hydrogen Adsorbents with High Volumetric Density: New Materials and System Projections*, 2016.
36 M. T. Kapelewski, T. Runcevski, J. D. Tarver, H. Z. H. Jiang, K. E. Hurst, P. A. Parilla, A. Ayala, T. Gennett, S. A. Fitzgerald, C. M. Brown and J. R. Long, *Chem. Mater.*, 2018, **30**, 8179–8189.
37 M. Dincă and J. R. Long, *J. Am. Chem. Soc.*, 2007, **129**, 11172–11176.
38 J. A. Mason, M. Veenstra and J. R. Long, *Chem. Sci.*, 2014, **5**, 32–51.
39 V. Kudiiarov, J. Lyu, O. Semenov, A. Lider, S. Chaemchuen and F. Verpoort, *Appl. Mater. Today*, 2021, **25**, 101208.
40 S. I. Kim, T. U. Yoon, M. B. Kim, S. J. Lee, Y. K. Hwang, J. S. Chang, H. J. Kim, H. N. Lee, U. H. Lee and Y. S. Bae, *Chem. Eng. J.*, 2016, **286**, 467–475.